COMPUTATION OF PERIODIC GREEN'S FUNCTIONS IN LAYERED MEDIA USING COMPLEX IMAGES TECHNIQUE

H. Bahadori, H. Alaeian, and R. Faraji-Dana

Center of Excellence on Applied Electromagnetic Systems
School of Electrical & Computer Engineering
College of Engineering, University of Tehran
P. O. Box 14395-515, Tehran, Iran

Abstract—In this paper, a new method based on the complex images technique has been presented to efficiently compute the Green's functions required in a Mixed Potential Integral Equation (MPIE) analysis of a periodic structure located on a layered medium. This method leads to a closed-form representation of the Green's functions of these periodic structures given in terms of slowly convergent series valid for sub-wavelength as well as super-wavelength cell sizes for all source-point to field-point distances. Comparison between the results obtained by the proposed method and those obtained through other numerical methods verifies its accuracy. Fast convergence, simple final form and versatility of the proposed method are its main advantages which make it suitable for the analysis of the periodic structures using the integral equation techniques.

1. INTRODUCTION

Periodic structures, such as electromagnetic or photonic band-gap (EBG/PBG) structures [1] and left-handed metamaterials (MTMs) with both negative effective permittivity and permeability [2] have been extensively developed and utilized through the last decade in order to control and manipulate the flow of the electromagnetic waves in various applications.

When applying numerical full wave methods such as integral equation techniques (IE) to periodic structures, fast and accurate means for evaluating the periodic Green's function are required.

While the application of the Floquet-Bloch theorem [3, 4] reduces the computational domain of infinite periodic structures to a single unit cell, it is still required to compute very slowly convergent series for their Green's functions like the magnetic vector potential and electric scalar potential Green's functions used in a conventional MPIE formulation. In order to speed up the evaluation of these series several acceleration techniques have been proposed in the literature which can be categorized in two main groups of the general algorithms and the specific ones.

Shank's [5], Chebyshev-Toeplitz, ρ [6], θ and Levin's transforms are some of the general algorithms while Kummer, Poisson [7] and Ewald's transforms belong to the second category. Among these methods Shanks' transformation can efficiently evaluate the periodic Green's function of planar stratified media, like the one shown in Fig. 1, but unfortunately its efficiency severely decreases when the field-source point distance diminishes.
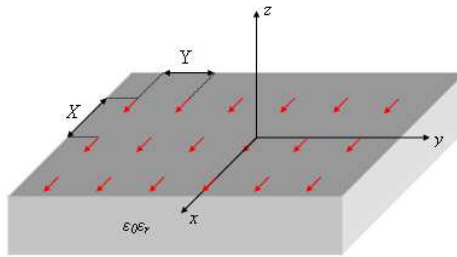
Figure 1. An infinite array of point sources above a substrate.

Ewald's transform [8] is another well-recognized technique in speeding up the summation of the periodic Green's function which partitions the main series into two spectral and spatial components with Gaussian decaying characteristics. In [9, 10], this method has been used to accelerate the convergence of the periodic Green's function series in free-space while in [11] it has been applied to the periodic Green's function of multilayered planar structures. However, the method shows some deficiencies in the evaluation of the complementary error functions with complex arguments. In [12], a new acceleration technique with exponential convergence rate has been presented, which is numerically less complex than Ewald's transform, easier to implement and performs better for moderate accuracies.

In [17], a combination of the Spectral Domain Approach (SDA) and the Array Scanning Method (ASM) was used to analyze a microstrip antenna located on a periodic metamaterial substrate.

When it comes to the layered media the complex image technique allows one to substitute the relevant Green's function with a finite summation of the free-space Green's functions [13]. Kipp and Chan [14] and Shubair and Chow [15] solved the problem of the periodic Green's function in layered media by using the acceleration techniques of the free-space periodic Green's function combined with the complex image technique.

In this paper, for the first time a simple, closed-form expression for the periodic spatial domain Green's function of a multilayered medium will be derived using the concept of complex images for multilayered media, leading to a summation of free-space Green's function, combined with the complex images representation of the periodic Green's function in free space presented in [16]. Using this method, it becomes possible to represent the Green's functions of arrays of periodic sources located on layered media in terms of finite summations of complex images. This representation is numerically more efficient than the other known techniques [14, 15, 17], as it avoids the computation of the infinite series. It is also valid for all the source-point to field-point distances.

On this ground, the paper first represents a brief introduction to the complex images technique in a multilayered medium that substitutes the main problem, i.e., an array of point sources over a layered medium, with a convenient array of sources located in homogeneous media. Then the method of complex images in periodic array of sources in free space will be reviewed and finally these two methods will be combined to complete the derivation of the proposed method in Section 2.

Numerical results will be presented in Section 3. There, the validity of the proposed method will be examined through different examples of 2-D periodic arrays of point sources over a grounded substrate. Finally Section 4 gives some concluding remarks.

2. FORMULATION OF THE PROBLEM

Assume a periodic array of point sources located above a layered medium (Fig. 1). In order to obtain the periodic Green's functions of such an array, we first consider an x-directed current source of unit-strength located above a layered medium as shown in Fig. 2. The $e^{j\omega t}$ time dependence is assumed throughout the paper. The spectral-domain MPIE potentials in the air region can then be obtained from the following equations:

$$\tilde{G}_A^{xx} = \frac{\mu_0}{4\pi} \frac{1}{j2k_{z0}} \left[e^{-jk_{z0}(z-z')} + R_{TE} e^{-jk_{z0}(z+z')} \right] \qquad (1a)$$
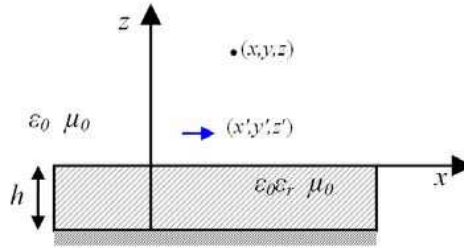
Figure 2. An x-directed electric source over a layered medium.

$$\tilde{G}_q = \frac{1}{4\pi\varepsilon_0}\frac{1}{j2k_{z0}}\left[e^{-jk_{z0}(z-z')} + (R_{TE} + R_q)\,e^{-jk_{z0}(z+z')}\right] \quad (1b)$$

where $k_{z0} = \sqrt{k_0^2 - k_\rho^2}$, and R_{TE} and R_q are the reflection coefficients from the layered medium defined in [13].

In (1), $\tilde{G}_A^{xx}$ represents the x component of the spectral-domain magnetic vector potential produced by the x-directed current source and $\tilde{G}_q$ is the spectral-domain electric scalar potential.

Using the procedure given in [13], one can extract the quasi-dynamic images [20] from the spectral domain representation (1) and write the following expressions for the spatial domain Green's functions by using the Sommerfeld's identity.

$$G_A^{xx}=G_{A0}^{xx}+\frac{\mu_0}{4\pi}\int\limits_{-\infty}^{+\infty}\frac{1}{j2k_{z0}}\,(R_{TE}-R_{TE0})e^{-jk_{z0}(z+\acute{z})}H_0^{(2)}\,(k_\rho\rho)\,k_\rho dk_\rho \quad (2a)$$

$$G_q=G_{q0}+\frac{1}{4\pi\varepsilon_0}\int\limits_{-\infty}^{+\infty}\frac{1}{j2k_{z0}}\,(R_{TE}+R_q-R_{TE0}-R_{q0})$$

$$e^{-jk_{z0}(z+\acute{z})}H_0^{(2)}\,(k_\rho\rho)\,k_\rho dk_\rho \quad (2b)$$

where R_{TE0} and R_{q0} are defined in [13] and

$$G_{A0}^{xx} = \frac{\mu_0}{4\pi}\left(\frac{e^{-jk_0r_0}}{r_0} - \frac{e^{-jk_0\acute{r_0}}}{\acute{r_0}}\right) \quad (3a)$$

$$G_{q0} = \frac{1}{4\pi\varepsilon_0}\left(\frac{e^{-jk_0r_0}}{r_0} + K\frac{e^{-jk_0r_0''}}{r_0''} + K^2\frac{e^{-jk_0r_1}}{r_1}\right.$$

$$\left. -K\frac{e^{-jk_0r_2}}{r_2} - K^2\frac{e^{-jk_0r_3}}{r_3} - K^2\frac{e^{-jk_0r_0'}}{r_0'}\right) \quad (3b)$$

$$r_0 = \sqrt{\rho^2 + (z - z')^2}, \quad r_0' = \sqrt{\rho^2 + (z + z' + 2h)^2}$$

$$r_0'' = \sqrt{\rho^2 + (z + z')^2}, \quad r_n = \sqrt{\rho^2 + (z + z' + 2nh)^2}, \quad K = \frac{1 - \varepsilon_r}{1 + \varepsilon_r}$$

By extracting the surface wave poles from the spectral domain Green's functions and approximating the remaining parts by a finite series of exponentials, using Prony's method [13] or other approximating techniques as GPOF [19], etc., a closed form representations of the spatial domain Green's functions are derived as [13]

$$G_A^{xx} = G_{A0}^{xx} + G_{A,ci}^{xx} + G_{A,sw}^{xx} \qquad (4a)$$

$$G_q = G_{q0} + G_{q,ci} + G_{q,sw} \qquad (4b)$$

where

$$G_{A,sw}^{xx} = \frac{\mu_0}{4\pi} (-2j\pi) \, Res_1 H_0^{(2)} (k_{\rho p}\rho) \, k_{\rho p} \qquad (5a)$$

$$G_{q,sw} = \frac{1}{4\pi\varepsilon_0} (-2j\pi) \, Res_2 H_0^{(2)} (k_{\rho p}\rho) \, k_{\rho p} \qquad (5b)$$

and

$$G_{A,ci}^{xx} = \frac{\mu_0}{4\pi} \sum_{i=1}^{N} a_i \frac{e^{-jk_0 r_i}}{r_i}, \qquad r_i = \sqrt{\rho^2 + (z + z' - jb_i)^2} \qquad (6a)$$

$$G_{q,ci} = \frac{1}{4\pi\varepsilon_0} \sum_{i=1}^{N} a_i' \frac{e^{-jk_0 r_i'}}{r_i'}, \qquad r_i' = \sqrt{\rho^2 + (z + z' - jb_i')^2} \qquad (6b)$$

Here, r_i and r_i' are the distances from complex images with amplitudes of a_i and a_i'. Also, $k_{\rho p}$ is a typical pole of the integrands in (2), giving contribution to the surface waves when determining the corresponding residue as in (5), and N is the number of exponentials used for the approximation of the spectral domain Green's functions which is normally between 3 to 7. In this way, a point source over a grounded substrate has been replaced by a number of real point sources (corresponding to G_{A0}^{xx} and G_{q0}) located in real locations in a homogeneous medium (ε_0), plus a number of point sources (corresponding to $G_{A,ci}^{xx}$ and $G_{q,ci}$) in complex locations with complex amplitudes located in again the same homogeneous medium ε_0, and a number of line sources (corresponding $G_{A,sw}^{xx}$ and $G_{q,sw}$) in the homogeneous medium with a relative permittivity of $\varepsilon_r = (k_{\rho p}/k_0)^2$.

Figure 3 visualizes the equivalence of the original problem (Fig. 2) with the combination of the two above-mentioned groups of point and line sources located in homogeneous media. Being able to replace the
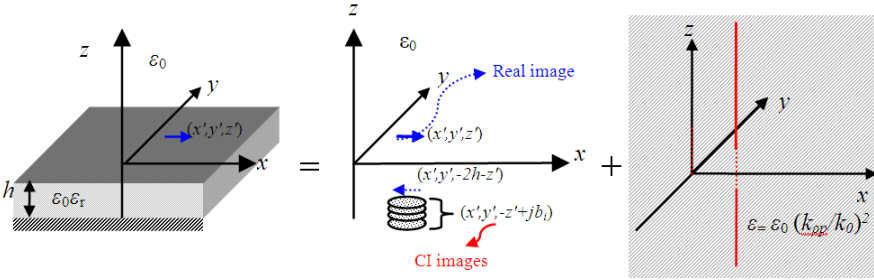
Figure 3. A visualization of different terms in (4a).

point source of Fig. 2 with a finite series of point and line sources located in homogeneous media as depicted in Fig. 3, paves the way to find the Green's functions of the periodic structure presented in Fig. 1 by considering each of these equivalent sources in an array configuration located in the respective homogenous medium.

To this end, first assume a 1-D periodic array of sources over a substrate. The Green's functions of this 1-D periodic structure are given by converting each term in (4) into a 1-D periodic array of sources located in homogeneous media. That is

$$G_{A-1D}^{xx} = G_{A0-1D}^{xx} + G_{A,ci-1D}^{xx} + G_{A,sw-1D}^{xx} \tag{7a}$$

$$G_{q-1D} = G_{q0-1D} + G_{q,ci-1D} + G_{q,sw-1D} \tag{7b}$$

where each term represents an infinite 1-D periodic Green's function corresponding to the periodic array of sources.

Without loss of generality assume an infinite array of point sources along x-axis as in Fig. 4 with X as the period of the array and k_x as the phase progression factor between two adjacent sources. Using the Floquet-Bloch theorem, the periodic Green's function, G^{per} is given by:

$$G_{1P}{}^{per} = \sum_{n=-\infty}^{+\infty} \frac{e^{-jk_0 r_n}}{4\pi r_n} e^{-jnk_x X}, \quad r_n = \sqrt{(x - nX)^2 + y^2 + z^2} \tag{8}$$

In [16], the complex images technique has been used to derive a closed-form representation for a 1-D periodic Green's function of point and line sources. Appendix A and B give a short description of the complex images formulation used to find the 1-D periodic Green's function of point and line sources, respectively. The final results are given by (17) and (21). It can be seen that instead of using a very slowly converging infinite series, one can use a finite series of complex images to compute the 1-D periodic Green's functions. Therefore the periodic
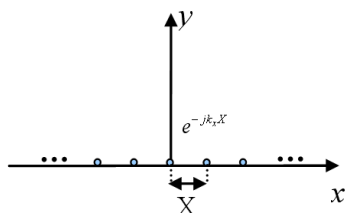
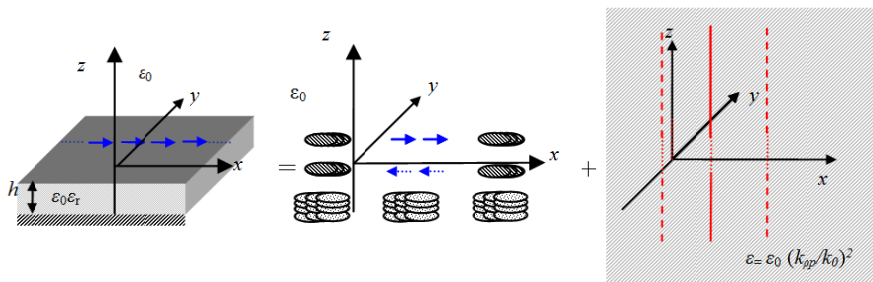**Figure 4.** A one-dimensional array of point sources.

Figure 5. A visualization of the complex image representation of 1-D array of point sources over a substrate.

Green's function of 1-D array of point sources over a substrate can be expressed in a closed-form, by some finite terms when the relevant periodic terms of (4) are substituted with their corresponding complex images representation of (17) and (21). Fig. 5 shows a visualization of the lattice of point and line sources in these two equations.

It is clear that G_{A0-1D}^{xx}, G_{q0-1D} and $G_{A,ci-1D}^{xx}$, $G_{q,ci-1D}$, must be computed by using (17) and $G_{A,sw-1D}^{xx}$, $G_{q,sw-1D}$ using (21). Here, the final form for one of the periodic terms of (7), i.e., G_{A0-1D}^{xx} is given as an example. Similar expressions can be easily written for the other terms.

$$
\begin{aligned}
G_{A0-1D}^{xx} = \frac{\mu_0}{4\pi} &\left(\frac{e^{-jk_0 r_0}}{r_0} - \frac{e^{-jk_0 r_1}}{r_1} + e^{-jk_x X} \frac{e^{-jk_0 r_{0x}}}{r_{0x}} - e^{-jk_x X} \frac{e^{-jk_0 r_{1x}}}{r_{1x}} \right. \\
&+ \sum_{n=1}^{N_1} a_n \left(\frac{e^{-jk_0 r_{0i}}}{r_{0i}} - \frac{e^{-jk_0 r_{1i}}}{r_{1i}} \right) \\
&\left. + e^{-jk_x X} \sum_{n=1}^{N_2} c_n \left(\frac{e^{-jk_0 r_{0xi}}}{r_{0xi}} - \frac{e^{-jk_0 r_{1xi}}}{r_{1xi}} \right) \right)
\end{aligned}
\tag{9}
$$

where r_1, r_2 are defined in (3) and:

$$r_{0x} = \sqrt{(x-X)^2 + y^2 + (z-z')^2}, \quad r_{1x} = \sqrt{(x-X)^2 + y^2 + (z+z'+2h)^2}$$

$$r_{0i} = \sqrt{(|x| + jb_n)^2 + y^2 + (z-z')^2},$$

$$r_{1i} = \sqrt{(|x| + jb_n)^2 + y^2 + (z+z'+2h)^2}$$

$$r_{0xi} = \sqrt{(|x-X| + jd_n)^2 + y^2 + (z-z')^2}$$

$$r_{1xi} = \sqrt{(|x-X| + jd_n)^2 + y^2 + (z+z'+2h)^2}$$

This idea can easily be extended to the case of 2-D periodic array of sources over a substrate where every source in Fig. 5 must be repeated with periodicity of Y, in y direction. Again the infinite series of sources in y direction can be reduced to finite series of sources by using (17) and (21), as in Fig. 6.
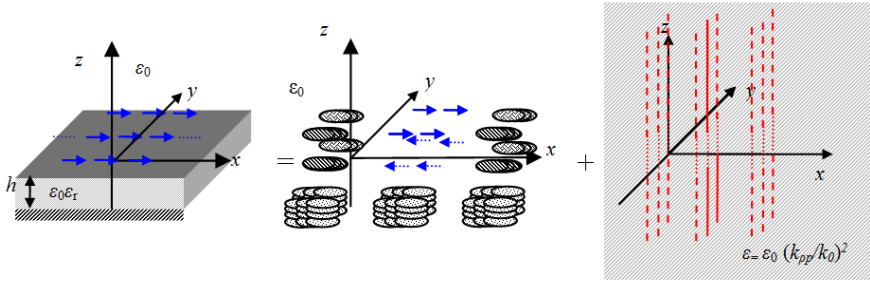
Figure 6. A visualization of the sources in complex images representation of 2-D periodic array of sources over a substrate.

This means that the periodicity of each term of G_{A0-1D}^{xx} and $G_{A,ci-1D}^{xx}$ or G_{q0-1D} and $G_{q,ci-1D}$ in y-direction can be expressed by some real point sources and other images in real or complex location of y-direction obtained from (17). While for y-direction periodicity of $G_{A,sw-1D}^{xx}$ and $G_{q,sw-1D}$ the complex image representation of (21) must be used.

It is worthy to notice that this method leads to a closed-form representation for the periodic Green's function of every kind of array and is valid for every source-field distance. In the representations the most effective elements of the array, i.e., sources surrounding the unit cell, will be preserved in their original form while images with complex amplitudes in complex locations model the behavior of all other sources in the array. So, the final representation can exactly

express the singularity of the Green's function near the boundaries. It also allows us to use some fewer terms when the near field values of the periodic Green's function are considered.

Finally, the method described in this section is quite general and applicable to any kind of array with any dimension but much simpler results can be obtained when special arrays are considered. Sub-wavelength arrays with periodicities less than the wavelength are one of those important arrays with simple complex image representation. In these arrays there exist no poles near the integration path shown in Fig. 12. Consequently the approximation process of (16) does not require the extraction of pole singularities of the respective functions. In these cases all the terms in the final representation resemble the original elements of the array except that they are complex valued elements in complex locations [18].

3. NUMERICAL RESULTS

In this section, the numerical accuracy of the developed method is demonstrated through various examples. For that purpose the magnitude and phase of the scalar and vector potentials of 2-D periodic arrays of sources over a grounded substrate have been obtained by using the proposed method and compared with ones obtained from relevant modal series accelerated with Shanks' transform. The arrays have been considered for both cases of sub and super-wavelength and
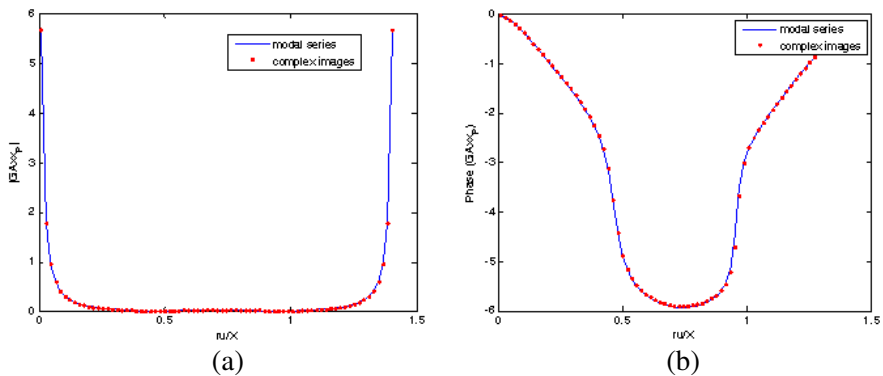

(a)   (b)
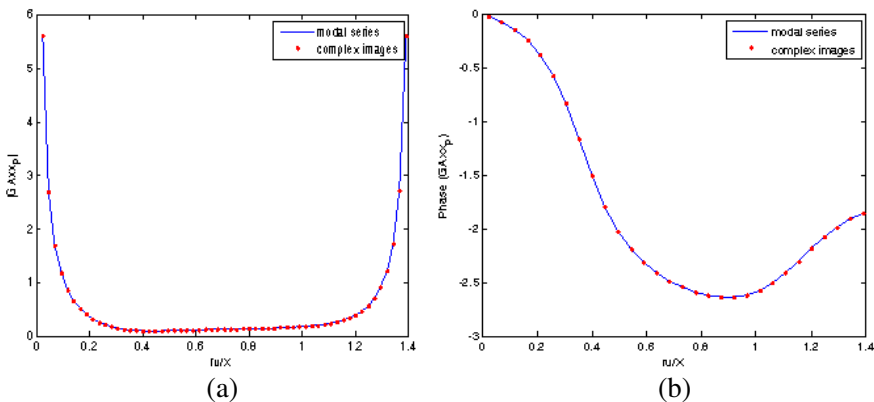
Figure 7. The vector potential of 2-D array of sources with $X = 0.6\lambda$, $Y = 0.6\lambda$, $k_x = \frac{\pi}{1.8\lambda}$, $k_y = \frac{\pi}{2.4\lambda}$ on a grounded substrate with $\varepsilon_r = 8.6$, $h = 0.06\lambda$ along its diagonal path in the unit cell (a) magnitude, (b) phase.

assumed to be located on a substrate with parameters of $\varepsilon_r = 8.6$ and $h = 0.06\lambda$. Throughout these examples the GPOF [19] method has been used in order to find the exponential approximations of (16) and consequent complex images.

Figures 7 and 8 show the results for vector and scalar potentials of a sub-wavelength 2-D array with $X = 0.6\lambda$, $Y = 0.6\lambda$, $k_x = \frac{\pi}{1.8\lambda}$, $k_y = \frac{\pi}{2.4\lambda}$, respectively. The observation point moves along the diagonal path in the unit cell. An excellent agreement can be observed between the two groups of results. The effect of poles and surface waves has been considered in this example.
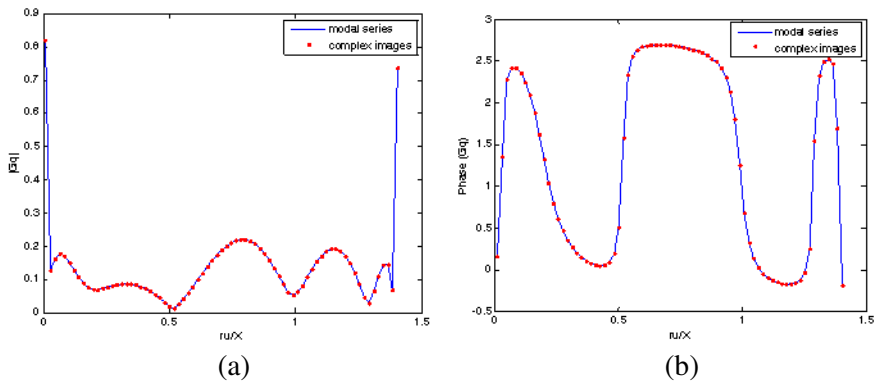

(a)   (b)
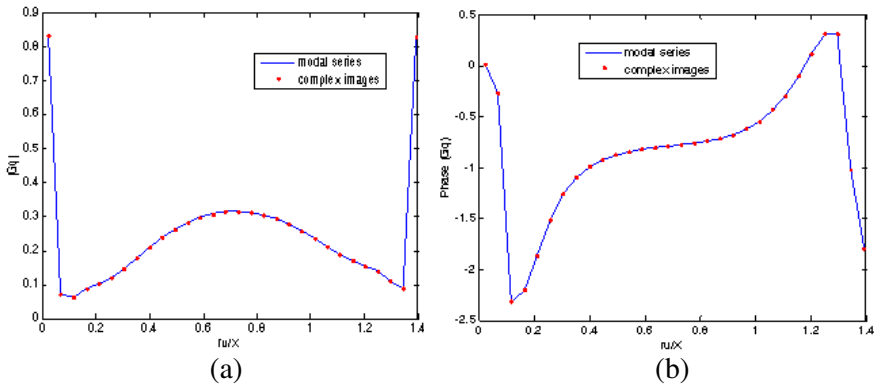
Figure 8. The scalar potential of 2-D array of sources with $X = 0.6\lambda$, $Y = 0.6\lambda$, $k_x = \frac{\pi}{1.8\lambda}$, $k_y = \frac{\pi}{2.4\lambda}$ on a substrate with $\varepsilon_r = 8.6$, $h = 0.06\lambda$ along its diagonal path in the unit cell (a) magnitude, (b) phase.



(a)   (b)

Figure 9. The vector potential of 2-D array of sources with $X = 1.5\lambda$, $Y = 1.5\lambda$, $k_x = \frac{\pi}{30\lambda}$, $k_y = \frac{\pi}{36\lambda}$ on a substrate with $\varepsilon_r = 8.6$, $h = 0.06\lambda$ along its diagonal path in the unit cell (a) magnitude, (b) phase.

Here, we have chosen $T_0 = 15$ (T_0 is the truncation point as shown in Fig. 12) and used 2 quasi-dynamic [20] and 6 complex image terms in (3) and (6) respectively to model the behavior of the grounded substrate. Also 4 complex images have been used in each direction of the periodic array in order to include the periodicity of the array.

Figures 9 and 10 represent the results of vector and scalar potential of a super wavelength 2-D array over the same substrate along the same path. Here, it has been assumed that $X = 1.5\lambda$, $Y = 1.5\lambda$ and $k_x = \frac{\pi}{30\lambda}$, $k_y = \frac{\pi}{36\lambda}$. Again excellent agreements are observed between the results of the two methods. Fig. 11 compares the magnitude of the

(a)   (b)

Figure 10. The scalar potential of 2-D array of sources with $X = 1.5\lambda$, $Y = 1.5\lambda$, $k_x = \frac{\pi}{30\lambda}$, $k_y = \frac{\pi}{36\lambda}$, on a substrate with $\varepsilon_r = 8.6$, $h = 0.06\lambda$ along its diagonal path in the unit cell (a) magnitude, (b) phase.
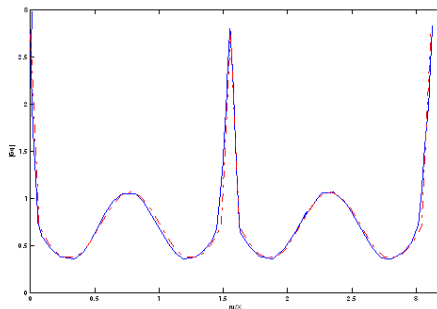
Figure 11. Magnitude of scalar potential of 2-D array of sources ($f = 30$ GHz, $X = Y = 1.1\lambda$, $k_x = k_y = 0$) over the substrate with $\varepsilon_r = 9.8$, $h = 0.06\lambda$ along its diagonal path of two unit cells. Our results are given by dashed line while the results of [15] are given in solid line.
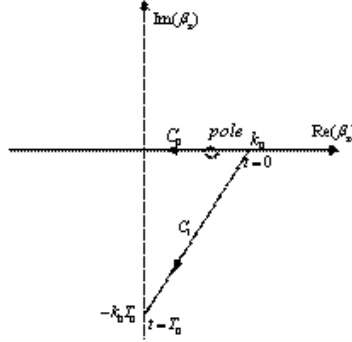
Figure 12. The approximation path in the β_x plane.

scalar potential of a 2-D array of sources in $f = 30\,\mathrm{GHz}$, $X = Y = 1.1\lambda$, $k_x = k_y = 0$ over the same substrate obtained using our proposed method with the results presented in [15] using Possion's transform accelerating technique. Again good agreement is observed.

4. CONCLUSION

In this paper, a novel method based on the complex images technique has been presented for the calculation of periodic Green's functions in layered media. Using this closed-form representation, fast and accurate computation of the periodic Green's function becomes possible for all the source-field points distances. This will drastically improve and facilitate the application of the integral equation techniques in analyzing the periodic structures and metamaterials.

APPENDIX A.

Consider a periodic array of point sources along the direction of x with period of X and phase shift of k_x. From the Floquet-Bloch theorem, the periodic Green's function G_{1P}^{per} is given by:

$$G_{1P}^{per} = \sum_{n=-\infty}^{+\infty} \frac{e^{-jk_0 r_n}}{4\pi r_n} e^{-jnk_x X} \tag{A1}$$

Using Sommerfeld's identity as:

$$\frac{e^{-jk_0 r}}{4\pi r} = \frac{1}{4\pi} \int_{-\infty}^{+\infty} \frac{e^{-j\beta_x |x|}}{j2\beta_x} H_0^{(2)}(k_\rho \rho) k_\rho dk_\rho \tag{A2}$$

where

$$\beta_x^2 + k_\rho^2 = k_0^2, \ \rho = \sqrt{y^2 + z^2}, \ r^2 = \rho^2 + x^2 \tag{A3}$$

after substituting (A2) in (A1) the periodic GF can be rewritten as:

$$G_{1P}^{per} = \frac{1}{4\pi} \int_{-\infty}^{+\infty} \sum_{-\infty}^{+\infty} e^{-jnXk_x} \frac{e^{-j\beta_x|x-nX|}}{2j\beta_x} H_0^{(2)} (k_\rho\rho) \, k_\rho dk_\rho \tag{A4}$$

The infinite integral of (A4) can be approximated with one along the truncated path of C_2 which can be replaced with C_1 according to the deformation theorem. Along this new path the geometrical series in the integrand of (A4) becomes a convergent one which its convergence limit is obtained from the following equations:

$$\sum_{n=-\infty}^{+\infty} e^{-jnXk_x} e^{-j\beta_x|x-nX|} = e^{-j\beta_x|x|} + e^{-jXk_x} e^{-j\beta_x|x-X|}$$

$$+e^{-j\beta_x|x|} \frac{e^{jX(k_x-\beta_x)}}{1 - e^{jX(k_x-\beta_x)}} + e^{-jXk_x} e^{-j\beta_x|x-X|} \frac{e^{-jX(k_x+\beta_x)}}{1 - e^{-jX(k_x+\beta_x)}} \tag{A5}$$

Substituting the above equation in (A4) the following results will be obtained:

$$\begin{aligned}
G_{1P}^{per} &= \frac{1}{4\pi} \int_{-\infty}^{+\infty} \frac{e^{-j\beta_x|x|}}{2j\beta_x} H_0^{(2)} (k_\rho\rho) \, k_\rho dk_\rho \\
&+ \frac{e^{-jXk_x}}{4\pi} \int_{-\infty}^{+\infty} \frac{e^{-j\beta_x} |x-X|}{2j\beta_x} H_0^{(2)} (k_\rho\rho) \, k_\rho dk_\rho \\
&+ \frac{1}{4\pi} \int_{-\infty}^{+\infty} \frac{e^{-j\beta_x|x|}}{2j\beta_x} \underbrace{\frac{e^{jX(k_x-\beta_x)}}{1 - e^{jX(k_x-\beta_x)}}}_{F_{1(\beta_x)}} H_0^{(2)} (k_\rho\rho) \, k_\rho dk_\rho \\
&+ \frac{e^{-jXk_x}}{4\pi} \int_{-\infty}^{+\infty} \frac{e^{-j\beta_x|x|}}{2j\beta_x} \underbrace{\frac{e^{-jX(k_x+\beta_x)}}{1 - e^{-jX(k_x+\beta_x)}}}_{F_{2(\beta_x)}} H_0^{(2)} (k_\rho\rho) \, k_\rho dk_\rho \tag{A6}
\end{aligned}$$

The first two terms correspond to the two most effective sources surrounding the unit cell. The last two terms can be simplified when the indicated fractions are approximated with exponential terms as below:

$$F_1 (\beta_x) = \sum_1^{N_1} a_n e^{b_n\beta_x}, \ F_2 (\beta_x) = \sum_1^{N_2} c_n e^{d_n\beta_x} \tag{A7}$$

Substituting the above equations in (A6), the following results will be obtained which leads to a closed-form representation for infinite

series in (A1):

$$
\begin{aligned}
G_{1P}^{per} &= \frac{1}{4\pi} \left(\frac{e^{-jk_0\sqrt{x^2+y^2+z^2}}}{\sqrt{x^2+y^2+z^2}} + e^{-jk_xX} \frac{e^{-jk_0\sqrt{(x-X)^2+y^2+z^2}}}{\sqrt{(x-X)^2+y^2+z^2}} \right. \\
&\quad + \sum_{n=1}^{N_1} a_n \frac{e^{-jk_0\sqrt{(|x|+jb_n)^2+y^2+z^2}}}{\sqrt{(|x|+jb_n)^2+y^2+z^2}} \\
&\quad \left. + e^{-jk_xX} \sum_{n=1}^{N_2} c_n \frac{e^{-jk_0\sqrt{(|x-X|+jd_n)^2+y^2+z^2}}}{\sqrt{(|x-X|+jd_n)^2+y^2+z^2}} \right)
\end{aligned} \tag{A8}
$$

In the case of a super-wavelength array, i.e., $X > \lambda$, there will exist one or more pole singularities close to the approximation path of Fig. 12. In this case the effect of these poles should be extracted from the approximated functions $F_1(\beta_x)$ and $F_2(\beta_x)$ and their effects should be added to (A8) by applying the residue theorem [18].

APPENDIX B.

The problem of 1-D periodic array of line sources is very similar to that of point sources except that (A1) and (A2) must be substituted with the following equations:

$$
G_{1L}^{per} = \sum_{n=-\infty}^{+\infty} \frac{e^{-jnXk_x}}{4j} H_0^{(2)}\left(k_0\sqrt{(x-nX)^2+z^2}\right) \tag{B1}
$$

$$
\frac{1}{4j} H_0^{(2)}\left(k_0\sqrt{x^2+z^2}\right) = \frac{1}{2\pi} \int_{-\infty}^{+\infty} \frac{e^{-j\beta_x|x|}}{j2\beta_x} e^{-jk_zz} dk_z \tag{B2}
$$

where

$$
\beta_x^2 + k_z^2 = k_0^2 \tag{B3}
$$

Substituting (B2) in (B1) and taking the same procedure as for point sources the following complex image representation will be obtained for 1-D array of line sources:

$$
\begin{aligned}
G_{1L}^{per} &= \frac{1}{4j} H_0^{(2)}\left(k_0\sqrt{x^2+z^2}\right) + \frac{e^{-jXk_x}}{4j} H_0^{(2)}\left(k_0\sqrt{(x-X)^2+z^2}\right) \\
&\quad + \sum_{n=1}^{N_1} a_n \frac{1}{4j} H_0^{(2)}\left(k_0\sqrt{(|x|-jb_n)^2+z^2}\right) \\
&\quad + e^{-jXk_x} \int_{n=1}^{N_2} c_n \frac{1}{4j} H_0^{(2)}\left(k_0\sqrt{(|x-X|-jd_n)^2+z^2}\right)
\end{aligned} \tag{B4}
$$

This completes the derivation of a closed form representation for periodic Green's functions of line sources.

REFERENCES

1. Maleki Javan, A. R. and N. Granpayeh, "Fast terahertz wave switch/modulator based on photonic crystal structures," *Journal of Electromagnetic Waves and Applications*, Vol. 23, No. 2–3, 203–212, 2009.

2. Khalilpour, J. and M. Hakkak, "S-shaped ring resonator as anisotropic uniaxial metamaterial used in waveguide tunneling," *Journal of Electromagnetic Waves and Applications*, Vol. 23, No. 13, 1763–1772, 2009.

3. Collin, R. E., *Field Theory of Guided Waves*, IEEE Press, New York, 1991.

4. Watanabe, K. and K. Yasumoto, "Accuracy improvement of the fourier series expansion method for floquet-mode analysis of photonic crystal waveguides," *Progress In Electromagnetics Research*, Vol. 92, 209–222, 2009.

5. Singh, S., W. F. Richards, J. R. Zinecker, and D. R. Wilton, "Accelerating the convergence of series representing the free periodic Green's function," *IEEE Trans. Antennas Propag.*, Vol. 38, No. 12, 1958–1962, Dec. 1990.

6. Singh, S. and R. Singh, "On the use of ρ-algorithm in series acceleration," *IEEE Trans. Antennas Propag.*, Vol. 39, No. 10, 1514–1517, Oct. 1991.

7. Jorgenson, R. E. and R. Mittra, "Efficient calculation of the free-space periodic Green's function," *IEEE Trans. Antennas Propag.*, Vol. 38, No. 5, 633–642, May 1990.

8. Papaniicolaou, V. G., "Ewald's method revised rapidly convergent series representations of certain Green's functions," *J. Comput. Anal. Applicat.*, Vol. 1, No. 1, 105–114, 1999.

9. Stevanovi'c, I., P. Crespo-Valero, K. Blagovic, F. Bongard, and J. R. Mosig, "Integral-equation analysis of 3-d metallic objects arranged in 2-D lattices using the Ewald transformation," *IEEE Trans. Microwave Theory Tech.*, Vol. 54, No. 10, 3688–3697, Oct. 2006.

10. Capolino, F., D. W. Wilton, and W. A. Johnson, "Efficient computation of the 2-D Green's function for 1-D periodic structures using the Ewald method," *IEEE Trans. Antennas Propag.*, Vol. 53, No. 9, 2977–2984, Sep. 2005.

11. Park, M. J. and S. Nam, "Efficient calculation of the Green's function for multilayered planar periodic structures," *IEEE Trans. Antennas Propag.*, Vol. 46, No. 10, 1582–1583, Dec. 1998.

12. Silveirinha, M. G. and C. A. Fernandes, "A new acceleration technique with exponential convergence rate to evaluate periodic Green's functions," *IEEE Trans. Antennas Propag.*, Vol. 53, No. 1, 347–355, Jan. 2005.

13. Chow, Y. L., J. J. Yang, D. G. Fang, and G. E. Howard, "A closed-form spatial Green's function for the thick microstrip substrate," *IEEE Trans. Microwave Theory Tech.*, Vol. 39, No. 3, Mar. 1991.

14. Kipp, R. A. and C. H. Chan, "A numerically efficient technique for the method of moments solution for planar periodic structures in layered media," *IEEE Trans. Microwave Theory Tech.*, Vol. 42, 635–643, Apr. 1994.

15. Shubair, R. M. and Y. L. Chow, "Efficient computation of the periodic Green's function in layered dielectric media," *IEEE Trans. Microwave Theory Tech.*, Vol. 41, No. 3, Mar. 1993.

16. Alaeian, H. and R. Faraji-Dana, "Accurate and fast computation of the Green's function of periodic structures using complex images technique," *2007 IEEE Antennas and Propagation International Symposium*, Honolulu, 2007.

17. Jarchi, S., J. Rashed-Mohassel, and R. Faraji-Dana, "Analysis of microstrip dipole antennas on a layered metamaterial substrate," *Journal of Electromagnetic Waves and Applications*, Vol. 24, No. 5–6, 755–764, 2010.

18. Alaeian, H. and R. Faraji-Dana, "A novel Green's function analysis of wave scattering by an infinite grating using complex images technique," *Applied Computational Electromagnetics Society (ACES) Journal*, Vol. 24, No. 5, 511–517, Oct. 2009.

19. Hua, Y. and T. K. Sarkar, "Generalized Pencil-of-Function method for extracting poles of an EM system from its transient response," *IEEE Trans. Antennas Propag.*, Vol. 37, 229–234, 1989.

20. Chow, Y. L., "An approximate dynamic spatial Green's function in three dimensions for finite length misrostrip lines," *IEEE Trans. Microwave Theory Tech.*, Vol. 28, 393–397, 1980.